sustainability

MDPI

Article

Assessment of Radionuclide Contamination in Foreshore Sands of the Baltic Sea near Juodkrante in Lithuania

Artūras Jukna [1,*] and Gražina Grigaliūnaitė-Vonsevičienė [2]

[1] Photovoltaic Technologies Laboratory, Department of Physics, Faculty of Fundamental Sciences, Vilnius Gediminas Technical University (Vilnius Tech), LT-10223 Vilnius, Lithuania
[2] Department of Physics, Faculty of Fundamental Sciences, Vilnius Gediminas Technical University (Vilnius Tech), LT-10223 Vilnius, Lithuania; grazina.grigaliunaite-vonseviciene@vilniustech.lt
* Correspondence: arturas.jukna@vilniustech.lt; Tel.: +370-5-251-2462

Abstract

This study presents a methodological approach to assess radionuclide contamination in the Baltic Sea near Juodkrante, Lithuania, based on measurements of β- and γ-emissions in seawater, foreshore sand, and dune top sand. Existing assessments often lack sufficient site-specific detail and multicompartment analysis, limiting the understanding of localized contamination and radionuclide behavior in coastal environments. Sampling was carried out between 2019 and 2024 at approximately the same geographical coordinates, along transects orientated normally to the shoreline. Given that the dune top remains unaffected by seawater intrusion, while the foreshore sand is subject to regular inundation, the foreshore environment is considered a natural filter that is capable of accumulating radionuclides from seawater. The proposed methodology supports the hypothesis that radionuclide retention in sandy substrates may persist beyond episodic contamination events in seawater, with retention dynamics influenced by environmental factors such as hydrodynamic conditions and aeolian processes. Simultaneous β- and γ-emission analysis enhances the precision of radionuclide quantification, while comparative evaluation of γ-spectra improves the detection of both natural and anthropogenic radionuclides, providing insight into both contemporary and historical contamination processes. The sustainability of the proposed approach lies in its efficient use of time, resources, and effort to monitor radionuclide contamination. Unlike conventional techniques that require energy-intensive seawater processing, this approach uses foreshore sand, which passively accumulates radionuclides through natural wave-driven deposition.

Keywords: Baltic Sea; seawater sustainability; radionuclides; foreshore sand; β-radiation; γ-ray spectroscopy

check for updates

Academic Editor: Guannan Liu

Received: 2 July 2025
Revised: 27 July 2025
Accepted: 13 August 2025
Published: 18 August 2025

Citation: Jukna, A.; Grigaliūnaitė-Vonsevičienė, G. Assessment of Radionuclide Contamination in Foreshore Sands of the Baltic Sea near Juodkrante in Lithuania. *Sustainability* **2025**, *17*, 7441. https://doi.org/10.3390/su17167441

Copyright: © 2025 by the authors. Licensee MDPI, Basel, Switzerland. This article is an open access article distributed under the terms and conditions of the Creative Commons Attribution (CC BY) license (https://creativecommons.org/licenses/by/4.0/).

1. Introduction

The study of radionuclide concentration and distribution in the marine environment is essential for assessing radiation exposure to living organisms from both natural and anthropogenic sources, and for evaluating potential health risks. Although water molecules can attenuate a portion of radiant energy [1], leading to the formation of species such as H_2, O_2, and H_2O_2 [2], thus reducing short-term exposure risks to biological organisms, radionuclides that occur in drinking water, dry soil, and air can pose serious health threats, as they possess sufficient energy to ionize atoms/molecules and damage living cells [3]. Therefore, monitoring the concentration of radionuclides in the marine environment is crucial to obtain

timely information on seawater contamination levels and the potential exposure of marine fauna, particularly when radiation doses can exceed the natural radioactive background.

Seawater quality studies are conducted worldwide by numerous research groups in both large and small water bodies, employing a variety of analytical methods [4]. An approach to simplifying the assessment of seawater quality involves monitoring changes in radioactivity levels within marine fauna, vegetation, or soil. However, such studies are often complex, costly, and may yield unreliable results, particularly in large aquatic systems, due to the migratory behavior of test subjects (e.g., fish or vegetation such as algae and other species), which can be influenced by water currents and wind patterns.

Among the world's largest water bodies, the Baltic Sea (estimated volume of 22,000 km^3) is recognized as one of the most radionuclide contaminated seas [5]. This pollution can potentially increase with the ongoing industrial development and the growing demands of the surrounding nations and populations. The Baltic Sea is continuously exposed to anthropogenic radionuclides discharged from nuclear power plants operating in the region [5,6], together with long-term contamination due to the release of radionuclides during the Chernobyl nuclear disaster [6]. The water of rivers and seawater from the North Sea slightly dilutes the water of the Baltic Sea [7]; however, the amount of water exchange per year is only approximately 3.5% of the total amount of seawater in the Baltic Sea. This rate of total water entry is not enough for the Baltic Sea to regenerate completely, even in several decades. Numerous research groups continuously monitor the concentration of radionuclides in the Baltic Sea, using methods to concentrate specific radionuclides from large volumes of seawater samples [8,9], as well as measuring and analyzing the γ-spectra of dried seawater samples [10]. However, seawater mixing processes caused by winds and currents [9], along with changes in water temperature, precipitates, and water salinity [9], lead to spatial and temporal variability in the radionuclide composition of samples collected from different areas and depths [11,12]. Therefore, to obtain high-quality monitoring results, samples must be collected multiple times from different areas and their radionuclide concentrations must be analyzed.

To improve the reliability of seawater quality monitoring and reduce the time required to assess variations in radionuclide concentrations with respect to sampling frequency and geographic coverage, this study proposes measuring and analyzing radioactive contamination of natural and anthropogenic origin in seawater, along with foreshore sand and dune top sand samples collected at the same time along a shore-normal transect. During stormy conditions, seawater flowing over the foreshore sand can deposit insoluble particles, including those to which radionuclides are adsorbed. This natural filtration process was investigated in 2019 and 2024 on the Baltic Sea foreshore near Juodkrante, Lithuania. In the Juodkrante region, with wave activity with average amplitudes ranging from 0.2 to 1.2 m [13] regularly floods the foreshore, the samples for the test were collected, over distances of approximately 3 to 20 m from the shoreline, respectively. As the waves retreat, a portion of the seawater returns directly to the sea, while the rest infiltrates the sand, allowing it to trap insoluble particles, including radionuclide-bound materials.

The primary objective of this study is to demonstrate that foreshore sand, with an average grain size of $(5.9 \pm 2.2) \times 10^{-4}$ m on the Baltic Sea coast near Juodkrante, Lithuania, can retain radionuclides from seawater even if sampling is carried out at approximately the same geographical coordinates, along transects orientated normal to the shoreline. The proposed method can improve the site-specific assessment and help to better understand localized contamination and the concentration of radionuclides accumulated in coastal areas. Additionally, it saves time and effort by reducing the need for multiple seawater samples from different locations, considering that long-term seawater dynamics are difficult to predict due to changing currents and winds. A comparative β- and γ-emission analysis

of seawater, foreshore sand, and dune top sand (unaffected by wave action) samples enables a more accurate assessment of both current (i.e., during the moment of sampling) and past (i.e., at a time when seawater samples were not taken for analysis) radionuclide concentrations. The proposed method might be used to assess radionuclide concentration in any large aquatic system; however, the current results are specific to the geographic area, where the efficiency of water filtering is influenced by the grain size of the foreshore sand, the costal slope, the amplitude of the waves, the frequency of the sea storm [13], and the water dynamics due to water streams. In this study, foreshore sand samples were collected from the dry sandy coast zone, which becomes submerged when wave amplitudes increased by approximately 10–20%, under minimal wave conditions corresponding to waves heights of 0.25 to 0.3 m. This sampling approach is important for the proper demonstration of this method, since it ensures effective interaction between the sand and seawater during elevated wave conditions [13] in Juodkrante, Lithuania. In addition, the proposed method is overall sustainable, as it reduces time, resource consumption, and operational effort. By utilizing foreshore sand, which naturally accumulates radionuclides through wave action, it eliminates the need for the energy-intensive procedures that are typical of conventional seawater sampling and preparation of samples for testing.

2. Samples and Methods

The samples for analysis were collected during the period between 2019 and 2024 at a site located at latitude 55°32′66.6″ N and longitude 21°07′33.3″ E on the Curonian Spit, a narrow strip of land separating the Curonian Lagoon from the Baltic Sea (Figure 1). This region forms part of an approximately 100 km long Lithuanian coastline along the Baltic Sea, of which only about 40 km directly face the open sea. Juodkrante, one of the villages situated along this stretch, is positioned with the Curonian Lagoon to its east and a sandy beach along the open Baltic Sea to its west.

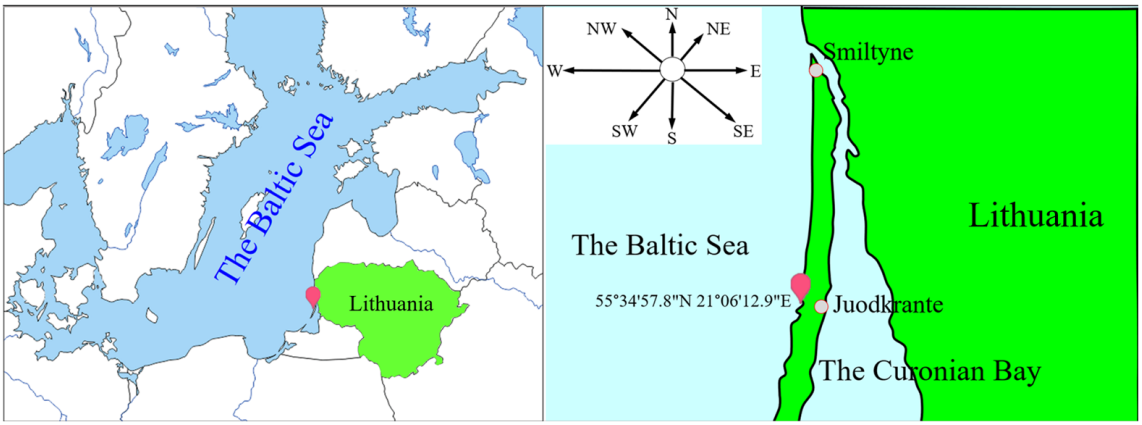

Figure 1. The location on the map (**left**) and the global coordinates of the sampling site (**right**). The inset at the top of the right panel indicates the prevailing wind direction and strength at the sampling site.

2.1. A Collection of Seawater Samples

All seawater samples in this study were collected under calm sea conditions, with wave heights not exceeding 0.3 m. The sampling was carried out at water temperatures ranging from 10 °C to 15 °C at a distance of 30 to 40 m from the shoreline along transects set perpendicular to the coast. Sample 1 (Figure 2, top) was always taken at sites with water depths of 1 to 1.5 m, preferably in visually clear water areas, minimally influenced by the backflow of turbulent return currents. For each sampling event, approximately 10 to 80 L of seawater were collected in plastic containers.

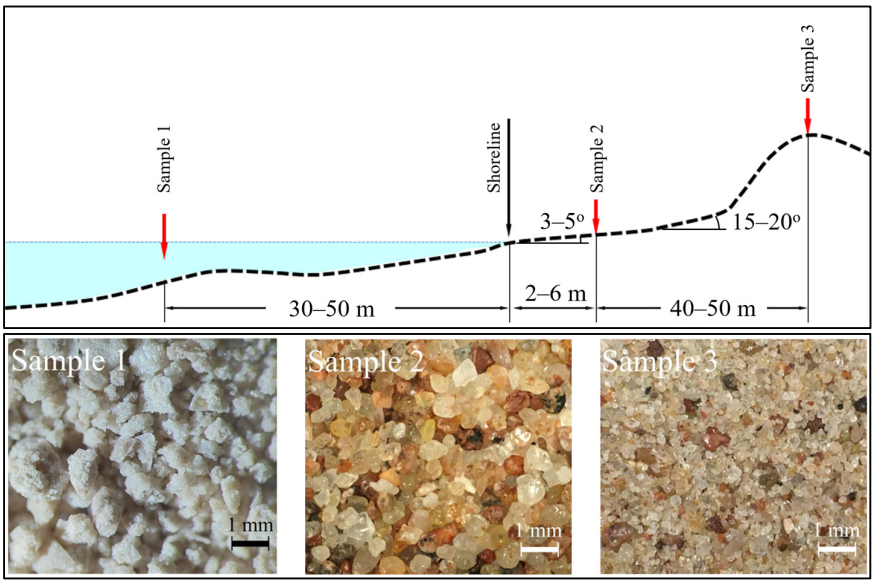

Figure 2. Schematic representation of the sample collection sites (**top**) and optical images of the corresponding samples (**bottom**): seawater residue (sample 1), foreshore sand (sample 2), and dune top sand (sample 3).

The seawater was then subjected to evaporation by boiling, resulting in the precipitation of dissolved salts along with a small fraction of sand particles. Subsequently, the solid residue was completely dried and further heated at temperatures between 230 °C and 250 °C to minimize the amount of intercrystalline water between and in the salt crystals. The resulting material exhibited an average grain size of $(7.3 \pm 4.2) \times 10^{-4}$ m, which is comparable to the grain sizes observed in the foreshore and dune top sand samples (samples 1–3 in Figure 2). Grain size measurements were performed using optical microscopy. Images of the ground crystals were obtained over an area of 225 mm^2, and grain sizes were calculated under the assumption that the crystal fragments were approximately spherical in shape.

2.2. A Collection of Sand Samples

The foreshore sand (sample 2 in Figure 2) of approximately 1 kg was collected during the period from 2021 to 2024 on the foreshore in the Juodkrante area, at a distance ranging between 1 and 7 m from the coast. Our optical microscope measurements revealed that the foreshore sand is characterized by an average grain size of $(5.9 \pm 2.2) \times 10^{-4}$ m.

Samples 2 and 3 were collected simultaneously on the day of sample 1 collection within a time interval of approximately 1 h. Importantly, each year, all three types of samples were collected along a shore-normal transect, at the average distances shown in Figure 2. At the site where the foreshore sand samples were taken, the beach had several slopes ranging from 3° to 5° near the shoreline, increasing to 15° to 20° near the dune. Based on visual observations, this place that ranged between 2 m and 6 m from the coast was flooded when the wave amplitude exceeded approximately 0.3–0.4 m, which is still considered not stormy sea conditions. When waves recede from the foreshore, part of the seawater returns with the receding wave, but the other part infiltrates the sand. During this infiltration process, insoluble particles, including those that contain adsorbed radionuclides, can be trapped among the sand grains.

At the site of sample 2 at the time of sample collection, the beach surface appeared to be dry. However, due to the low slope of the beach (approximately 3° to 5°) and the relatively short distance of 2 to 6 m from the coast, the foreshore sand was found to be wet from depths of 0.1 m and continuing down throughout the sampling depth. In cases where

multiple samples of sample 2 type were taken at different depths, each individual sample was made to contain sand from an approximately 0.2 m depth interval.

This observation suggests that when the wave recedes during a storm, infiltration of insoluble particles among the sand grains can be expected at depths starting from 0.1 m. Additionally, as the wave subsides, some portion of the fine sand fraction can be washed out from the foreshore surface and carried by streams to new locations. The rate of sand removal and its return to the foreshore depends on the direction of the wind and water streams. Based on the investigation of the dynamics of the concentration of ^{137}Cs radionuclides in marine sands [14], a sand layer up to 0.4 m thick can be washed away from the foreshore into the sea during storms and subsequently returned to the foreshore at other locations, contributing to the continued alteration of the Baltic Sea coastline. This change in coastline is also influenced by the ongoing rise in seawater levels [15]. Since 1980, this phenomenon has resulted in an average rate of approximately 2.6 ± 0.65 mm per year, as summarized by various research groups and measurement methods [15,16]. An annual increase in water level causes coastal erosion, leading to a continual shortening of the foreshore. Since foreshore sand samples were collected once per year, each time we choose an area where the total length of the foreshore was as long as 40–50 m and had a similar slope of the foreshore in a range between 3° and 5° near the coast (Figure 1), and we choose the dry surface of the foreshore, with the distance from the coast at which the foreshore sand becomes wet starting at depths of approximately 0.1 m and continuing throughout the entire sampling depth.

The sand on the top of the dune (sample 3), collected at distances of 40 to 50 m from the coast and at an altitude of approximately 5 or 7 m above sea level, was never flooded by seawater. Therefore, the radionuclides from seawater cannot directly reach the top of the dune. Copplestone et al. [17] and Druteikiene et al. [18] suggested that the accumulation of radionuclides in the sand of the beach is mainly due to their transfer from the sea to land. They are bound to marine sediments or fine particles and can be transported to the surface microlayer by rising air bubbles. There, they may be released into spray droplets and become airborne aerosols, particularly in the surface, where breaking waves enhance bubble production [17]. Moreover, the surface zone appears to be the main area for generating radionuclide-contaminated sea spray and that in winds up to 10 m/s, radionuclides in sea spray can be derived from sediment suspended in seawater in the surf zone [19]. The later work of the same research group confirmed that radionuclides in seawater can originate from direct discharges of radioactive material to the sea and be bound to particulates sinking to the seabed. However, during storms, the remobilization and horizontal or vertical transport of the sediment can rise up and be carried by waves to the foreshore sand.

Radionuclide concentration at the top of the dune can originate from natural sources (owing to the presence of long-lived radionuclides) and from anthropogenic radioactive material discharges into seawater, the atmosphere, or via the aeolian transport of sand from the coast soil or adjacent dunes [17–20]. Since the concentration of radionuclides on the dune top is much lower compared to the change in the seawater, the dune top sand was used as a reference sample in our measurements.

Similarly to the procedure applied for sample 2, the grain size analysis of the sand collected on top of the dune was carried out using optical microscope images. The analysis revealed an average grain size of $(2.4 \pm 1.1) \times 10^{-4}$ m, assuming that the sand grains in sample 3 are approximately spherical in shape. Table 1 presents a summary of the characteristics of the three types of samples collected during the period of 2019–2024.

Table 1. Summary of the characteristics of the three sample types collected during the period of 2019–2024: seawater (sample 1), foreshore sand (sample 2), and dune top sand (sample 3).

Sample	Sampling Date	Average Grain Size, $\times 10^{-4}$ m	Sample Mass, g	Seawater Volume, L	Distance [1] from Coast, m	Depth [2], m	Height [3], m
Sample 1	15 June 2019	7.3 ± 4.2	26.5	10	34–36	0.7–1.0	-
	30 May 2020		77.6	9.55	37–39	0.7–1.0	-
	9 June 2021		320.4	44.47	36–38	0.7–1.0	-
	14 June 2022		397.9	55	28–32	0.7–1.0	-
	19 May 2023		355.4	42.52	34–36	0.7–1.0	-
	17 June 2024		558.2	78.74	41–43	0.7–1.0	-
Sample 2	15 June 2019	-	-	-	-	-	-
	30 May 2020	-	-	-	-	-	-
	9 June 2021	5.9 ± 2.2	1352.7	-	3.0–3.5	0.00–0.20	-
	14 June 2022		1007.8	-	5.0–5.5	0.00–0.20	-
	19 May 2023		1060.0	-	5.0–5.5	0.20–0.40	-
			1186.4	-	5.0–5.5	0.40–0.60	-
			1055.3	-	6.5–7.0	0.00–0.20	-
			1022.5	-	6.5–7.0	0.20–0.40	-
			1089.1	-	6.5–7.0	0.40–0.55	-
			1389.9	-	6.5–7.0	0.50–0.65	-
	17 June 2024		1110.6	-	1.0–1.3	0.00–0.20	-
		-	1705.2	-	27–28	0.00–0.20	1.5–2.5
Sample 3	15 June 2019	-	-	-	-	-	-
	30 May 2020	-	-	-	-	-	-
	9 June 2021	2.4 ± 1.1	1452.9	-	20–22	0.00–0.20	6.0–7.0
	14 June 2022		1178.8	-	48–50	0.00–0.20	7.0–8.0
	19 May 2023		1131.2	-	39–41	0.00–0.20	6.0–7.0
	17 June 2024		1522.3	-	50–52	0.00–0.20	4.8–5.0

[1] For sample 1, the distance is measured from the coastline toward the sea, whereas for samples 2 and 3, it is measured landward towards the dune along a normal to coastline. [2] For sample 1, depth refers to the sampling depth in the marine environment. For samples 2 and 3, it indicates the average depth from the surface at which the sand was collected. In cases of multiple samples (sample 2) at the same distance from the coast, each individual sample was made to contain sand from an approximately 0.2 m depth interval. [3] Approximate elevations of the dune crests at the sample collection site above sea level.

The column "Depths" in Table 1 indicates the depth at which the seawater sample (sample 1) was collected and/or the depth at which the sand sample (sample 2) was taken. The rationale for collecting sand samples from below the surface is to assess the extent to which radionuclides from past contamination events have penetrated the sediment. This helps to assess the need to sample deeper sand layers to reconstruct the historical record of marine pollution. The underlying assumption is that sand can act as a natural filter, where radionuclides may adsorb onto sand grains as wave-driven water recedes back into the sea.

2.3. Procedures for the Preparation of Dried Seawater and Sand Samples

To remove residual water from salt crystals in dried seawater and sand samples, the samples were annealed at a temperature of 250 to 270 °C (furnace-indicated temperature) in a dry air atmosphere under an atmospheric pressure of 1 atm. Following annealing, the samples were gradually cooled for a period of 60 to 80 min to a final temperature of 40 to 50 °C. At 250 °C, water molecules exhibit high kinetic energy, enhancing their ability to escape into the gaseous phase from the salt crystal lattice (sample 1), the pores within the sand grains (samples 2 and 3), and from large crystal aggregates formed in sample 1 during the initial drying process [21]. Crystallized salt on the surface of the sand grains makes it difficult for water to evaporate at lower temperatures, as water molecules strongly

interact with the dissolved salt ions [21,22]. According to Ref. [21], variations in the flow of water diffusion from and through the granular sand matrix are associated with reduced compaction and increased porosity in both the sand and dried seawater samples, leading to a general increase in sample volume.

Following annealing, the salt crystals were milled to obtain a particle size that was comparable to that of the sand grains. This ensured that all tested samples underwent the same preparation procedures, promoting uniformity throughout the set samples.

The residual water content in the seawater and sand samples was estimated by measuring the mass of the sample before and after thermal drying. The percentage of mass loss, attributed to water evaporation, was calculated using the following expression: $M_s = 100\% \times (m_0 - m)/m$. Here, M_s is the relative mass loss, m_0 is the initial mass, and m is the final mass after heating. Prolonged exposure of the samples to ambient air resulted in an increase in mass as a result of the absorption of atmospheric moisture. This mass gain ranged from approximately 0.48% to 0.69% per hour, depending on the average grain size [23] and the duration of exposure to air. To minimize post-annealing moisture absorption by salt crystals (sample 1) and sand grains (samples 2 and 3), all samples, while still at a temperature of 40 to 50 °C, were immediately transferred to an SBT-13 end-window beta counter for beta radiation measurements or sealed in a moisture-resistant container for gamma spectrometry.

The application of identical thermal treatment conditions across all samples probably ensured the evaporation of volatile radionuclides and/or their precursors. Consequently, only nonvolatile radionuclides are expected to remain after the annealing of the samples, allowing for their identification and quantification through the analysis of their radioactivity.

2.4. Measurements Setup for Registration of Gamma-Ray Emission

The prepared samples were measured using a portable spectrometer (Canberra InSpector 1000 IN1K Portable Gamma Detector, Mirion Technologies (Canberra UK) Ltd., Newbury, UK), equipped with an integrated preamplifier and a sodium iodide (NaI(Tl)) scintillation detector (IPROS-3_v1, Mirion Technologies (Canberra UK) Ltd.) featuring a crystal of dimensions of 76 × 76 mm^2). The spectrometer operates at ambient temperature. Gamma-ray spectra were recorded using a 512-channel multichannel analyzer, covering an energy range from 25 to 3000 keV, with an approximate energy resolution of 5–6 keV per channel. According to the manufacturer's specifications, the instrument exhibits a sensitivity to ^{137}CS of 32,000 cps/mrem/h ± 3.5%. The energy calibration of the system follows a linear relationship defined by the following equation, $E = 10.23 + 0.4567 \times C_N$, where E is the energy in keV and C_N is an integer index corresponding to the channel number of the detection system.

The calibration of the energy scale was performed using the well-known gamma emission line of the radionuclide ^{40}K, which exhibits the most prominent peak in all measured spectra of the sand samples. Specifically, the observed ^{40}K peak, originally recorded at 945.102 keV, was shifted to align with its characteristic energy of 1460.80 keV. This correction led to an expansion of the entire spectrum toward higher energy values. The full width at half maximum (FWHM) of the peak amplitude was calculated using the following empirical formula:

$$FWHM = 0.9871 + 0.03463 \times E^{1/2} \quad (1)$$

where E is the energy in keV. The peak tailing was characterized by the following expression:

$$T_p = 1.127 + E \times 2.053 \times 10^{-4} \quad (2)$$

The calibration of efficiency for radionuclide detection (*Eff*) was performed by applying polynomial fits to the spectra, achieving a fit accuracy better than 4.9% relative to the experimental data. For the energy range (0–2500 keV), efficiency was calculated using the following polynomial:

$$Eff = \exp\left[-7.969 + 1.196 \times \ln(E) - 0.1442 \times \ln(E)^2\right] \quad (3)$$

Since the detection efficiency of a gamma line depends on the energy position of each identified peak within the gamma spectrum, the measurement uncertainty is evaluated using Equation (3). By taking the energy interval per channel as a parameter, the uncertainty in the energy calibration can be estimated, based on principles of statistical physics, as two thirds of the channel width. However, in practice, this uncertainty is computed by the spectrometer software (Genie 2000. Gamma Acquisition & Analysis V3.2.1. 26 August 2009, by Canberra Industries, Dover, NJ, USA) and reported in the datasheet in the Nuclide Identification Report section (see Supplementary Materials). On average, the activity arising from the counting statistics is less than ±5%.

The background contribution to the gamma spectra was removed using a standard background subtraction procedure implemented in the spectrometer analysis software (Genie 2000. Gamma Acquisition & Analysis V3.2.1. 26 August 2009, by Canberra Industries).

To ensure greater precision in the measurement results, each gamma spectrum for samples 1–3, collected during the period of 2021 to 2024, was recorded over approximately 20 h using the experimental setup shown in Figure 3. A nearly identical volumetric amount of the test material was poured into a plastic container with the spectrometer probe positioned at its center. In all measurements, the material formed an approximately 2 cm thick layer (highlighted in yellow) surrounding the cylindrical body of the spectrometer probe, with a contact surface area of 852 cm^2 (highlighted in red). Both the sample and the probe were wrapped in a protective film to prevent the diffusion of environmental water vapor. The assembly was then placed inside a shielding chamber with lead walls that exceeded 10 cm in thickness, effectively attenuating ambient gamma radiation.

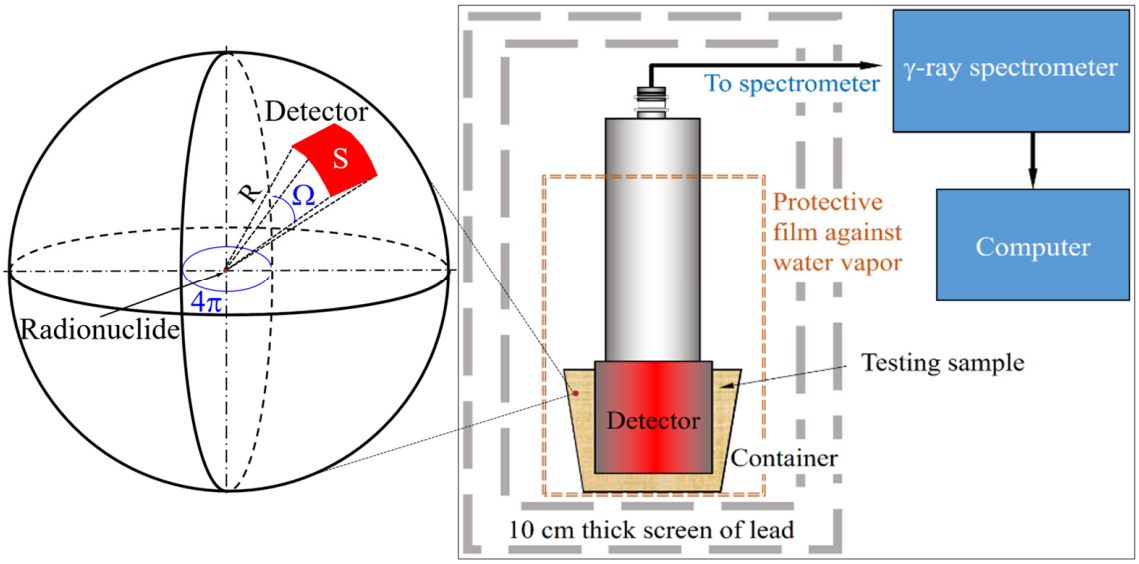

Figure 3. A test sample (highlighted in yellow), at a temperature of approximately 40–50 °C, was poured into a container such that a layer of the test material at least 2 cm thick surrounded the probe (highlighted in red) of the gamma spectrometer (**right**). The inset (**left**) presents a schematic illustration of the radionuclide radiation incident on the detector surface *S* within a solid angle Ω.

Each radionuclide (inset in Figure 3) is a point source of radiation, radiating with the same probability at a space angle of 4π. According to our estimations, for the circular probe of the gamma spectrometer with radius r = 38 mm and height h = 76 mm of the cylinder, the approximation of the solid angle at which the flat face of the probe cylinder faces the radionuclide located at distance R is given as follows:

$$\Omega(R) = 2\pi\left(1 - \frac{R}{\sqrt{R^2 + r^2}}\right) \quad (4)$$

The values of $\Omega(R)$ for the range of distances 10 mm $\leq R \leq$ 20 mm falls between 2.82 and 3.62 sr. For the purpose of estimating the total gamma radioactivity of each sample, an average solid angle of $\Omega \approx 3.27$ sr was used. Furthermore, maintaining comparable sample volumes and similar grain sizes of salt and sand in all three types of samples allowed for consistent measurement conditions. This consistency allows for a reliable comparison of gamma spectra across a wide energy range, facilitating the identification of radionuclide types and the determination of their concentrations in samples 1 to 3.

2.5. Measurement Setup for Registration of Beta-Ray Emission

Beta radioactivity measurements were performed on three types of samples (as detailed in Table 1), and for each measurement, a defined portion of the sample was placed in a container with internal dimensions of 3.5 × 5.0 × 0.7 cm^3. In the case of a full container, the surface of the sample appears to be in close proximity to the mica window of the detector, resulting in a distance of approximately 10 mm from its anode. In this case, the mass of the dried seawater sample (sample 1) ranged from 10.52 to 11.50 g, while the masses of the dried sand samples (samples 2 and 3) were within the range of 17.52 to 20.81 g. To ensure greater reliability and precision in the measurements of beta activity, all samples were thermally pretreated in ambient air at 200 °C for 10–15 min. This annealing process was used to remove residual moisture, both absorbed and adsorbed, that could otherwise affect the results. For repeated measurements, this moisture removal procedure was repeated before each measurement to maintain consistent sample conditions. The non-portable experimental setup used for the beta radiation measurements, shown in Figure 4, is based on the SBT-13 beta scintillation counter. This instrument is designed to measure the count rate of low-energy (soft) beta radiation.

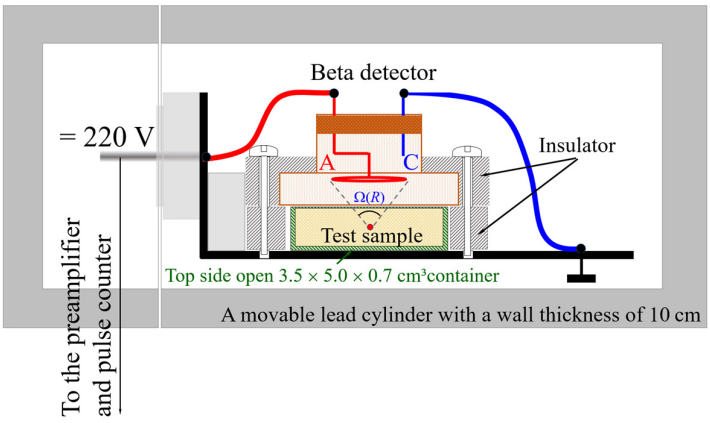

Figure 4. The test sample (yellow), which was at a temperature of 40 to 50 °C, was poured into a rectangular container (green) with dimensions of 3.5 × 5.0 × 0.7 cm^3 and integrated into the SBT-13 beta counter system. A and C indicate the anode and cathode of the detector, respectively. To reduce the impact of the environment, the entire assembly was enclosed in a movable lead cylinder. The solid angle $\Omega(R)$, through which radiation from a radionuclide reaches the detector, depends on the distance R between the radionuclide and the detector.

Being a minimal distance from the mica window of the beta detector, the surface of the test sample was approximately 10 mm from its anode A (Figure 4). To reduce the impact from the environment, the entire assembly was enclosed in a 100 mm thick lead shield cylinder. The solid angle Ω, through which radiation from a radionuclide reaches the detector, depends on the distance *R* between the radionuclide and the detector. This device features a large 30 mm diameter mica window, enabling the detection of low-energy particles, and operates at 220 V for beta radiation measurement in the samples. According to the manufacturer's specifications, the beta counter has a sensitivity in the range of 100 to 140 counts per second (cps), a dark count rate of 0.6 cps, and a detection efficiency of $\eta_\beta = 0.3$.

To ensure greater precision of measurement, each test sample was measured 2–3 times over a period of at least 4 to 7 h, with beta counts recorded approximately every hour. This approach allowed for the estimation of deviations from the average count rate, which were associated with an increase in the absorbed water content in the samples. The ionization of water molecules by high-energy electrons and positrons (i.e., radiolysis) can significantly attenuate beta radiation due to partially blocking beta particles emitted from radionuclides [24]. Therefore, in our multiple experiments, a deviation for more than 10% from the average value of the first results was not included and analyzed in the present study.

3. Results and Discussion

Figure 5 shows a gamma-ray spectrum of foreshore sand (sample 2) measured over the energy range of 23.27 to 1659.1 keV. The spectrum was recorded over a duration of 19 h and 53 min, corresponding to a total acquisition time of 71,580 s. The observed peaks in the spectrum are relatively broad, with the FWHM ranging from 10 to 30 keV. Most of the identified peaks consist of closely spaced peaks that partially overlap each other. Consequently, determining their amplitudes and FWHM requires computational analysis using the dedicated software of the gamma spectrometer (Genie 2000. Gamma Acquisition & Analysis V3.2.1. 26 August 2009, by Canberra Industries).

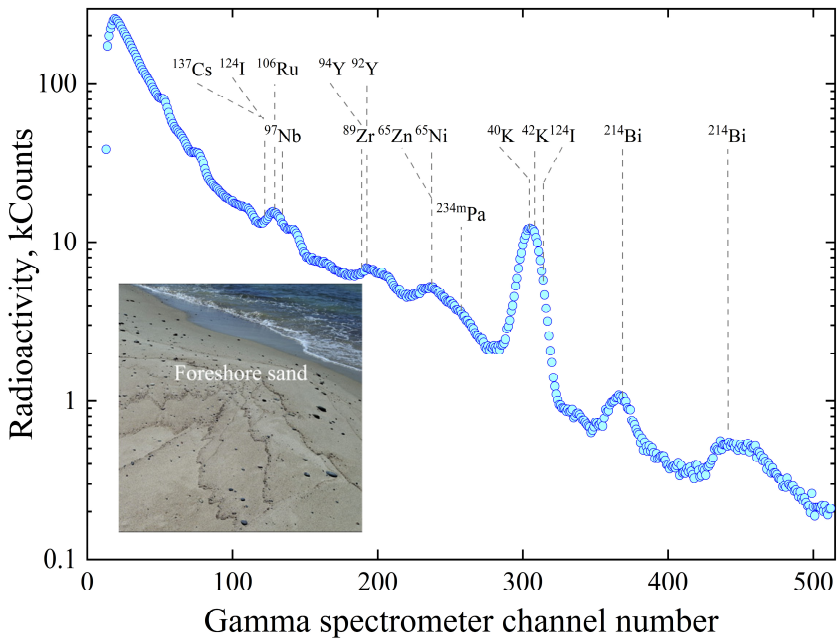

Figure 5. The gamma spectrum of the foreshore sand (sample 2) collected in Juodkrante in June 2021.

The spectrum exhibits a characteristic gamma emission line of the radionuclide potassium ^{40}K at 1460.8 keV, which represents the most intense peak observed. Due to its high intensity, this peak was employed for energy calibration across the spectra of all analyzed samples. The rest of the spectra and results of analysis carried out by the gamma spectrometer's software (Genie 2000. Gamma Acquisition & Analysis V3.2.1. 26 August 2009, by Canberra Industries) are provided in the Supplementary Materials.

3.1. Determination of Radionuclide Gamma Activity in Samples Based on Characteristic Gamma-Ray Emission Spectral Lines

Table 2 summarizes the identified radionuclides and their corresponding specific gamma activities A_γ in the sample estimated from spectral gamma emission lines of samples 1 to 3, collected in the Juodkrante region during the summer of 2021. The masses of the samples, along with other relevant parameters necessary for the evaluation of A_γ, for each radionuclide, are provided in Table 1. The identification confidence values (id confidence) in Table 2 indicate the likelihood that the observed gamma emissions originate from a given radionuclide, as determined by the spectrometer software. Dashes indicate radionuclides not identified in a given sample.

The gamma spectra of the three samples revealed approximately thirteen identifiable radionuclides, each characterized by a corresponding identification coefficient (id coefficient), as summarized in Table 2. The value of this coefficient, which ranges from 0 to 1, quantifies the probability that the software has accurately attributed a specific gamma emission peak to a particular radionuclide. The highest identification confidence values were recorded for radionuclides with comparatively long half-lives, notably ^{40}K, ^{65}Zn, ^{106}Ru, ^{124}I, and ^{137}Cs. The gamma-specific activities of the identified radionuclides A_γ were estimated from their corresponding spectral lines using the following expression:

$$A_\gamma = \frac{\text{Counts/time}}{Eff \times Yield}, \quad (5)$$

Here, *Yield* (Table 2) denotes the probability that a gamma photon of a specific energy is emitted per the disintegration of this radionuclide. A comparison of the calculated radionuclide gamma activities A_γ in all three samples reveals that the highest values are observed in the dried seawater sample for nearly all identified radionuclides (Table 2). For example, the activity of the ^{40}K radionuclide per 1 g in sample 1 is 3.69 times higher than that in sample 2 and 4.39 times higher than that in sample 3. In particular, the activity in sample 2 also exceeds that in sample 3. This result supports our hypothesis that foreshore sand located near the coastline can accumulate higher concentrations of radionuclides due to frequent inundation by seawater transported by waves.

Assuming that sample 1 was prepared using 44.47 L of seawater (Table 1), this allows for an estimation of the specific activity of ^{40}K in seawater as approximately 6.7 Bq/L. The obtained value is close to that assessed by other research groups [25], assuming that the distribution of radionuclides in seawater is dependent on seawater salinity, and river water inlet and seasonal water mass dynamics [25,26].

Table 2. Gamma-specific activities A_γ in the samples (Bq·g^{-1}) of dried seawater (sample 1), foreshore sand (sample 2), and sand from the top of a dune (sample 3) collected in the Juodkrante region in June 2021.

				Sample 1			Sample 2			Sample 3		
Radionuclide	**Energy, keV**	**Half-Life, $T_{1/2}$**	***Yield* *, %**	**Id Confidence**	**Counts ****	**A_γ, Bq·g^{-1}**	**Id Confidence**	**Counts ****	**A_γ, Bq·g^{-1}**	**Id Confidence**	**Counts ****	**A_γ, Bq·g^{-1}**
^{40}K	1460.80	1.25×10^9 y	10.67	0.999	21,190	0.927	1.000	24,187	0.251	0.999	21,860	0.211
^{42}K	1524.67	12.36 h	17.90	0.859	20,950	0.952	-	-	-	0.859	21,630	0.217
^{65}Ni	1115.52	2.517 h	14.80	0.711	12,336	0.427	0.695	21,179	0.174	0.711	13,261	0.101
	1481.84		23.50		52,799	2.339		60,347	0.633		54,575	0.533
^{65}Zn	1115.52	244 d	50.75	0.916	656	0.023	0.884	1126	0.009	0.916	704	0.005
^{89}Zr	909.10	78.4 h	99.04	0.868	271	0.008	-	-	-	0.869	295	0.002
^{92}Y	934.46	3.54 h	13.90	-	-	-	0.483	9857	0.070	-	-	-
	1405.40		4.80	-	-	-		213,749	2.138	-	-	-
^{94}Y	918.80	18.6 m	56	0.665	19,407	0.575	0.639	27,221	0.191	0.666	21,142	0.138
	1138.90		5.99		245,421	8.643		421,430	3.515		263,847	2.049
^{97}Nb	657.90	72.1 m	98.09	0.968	3002	0.070	0.976	2889	0.016	0.974	3001	0.015
	1024.50		1.08		260,998	8.428		366,078	2.800		284,308	2.025
^{106}Ru	621.84	373.59 d	9.80	0.793	2622	0.059	0.790	2521	0.013	0.791	2616	0.013
^{124}I	602.71	4.18 d	59.00	0.642	466	0.010	0.634	448	0.002	0.637	465	0.002
	1509.49		2.91		83,139	3.746		94,905	1.013		85,803	0.852
^{137}Cs	661.65	30.17 y	85.12	0.960	301	0.007	0.969	290	0.002	0.967	301	0.002
^{214}Bi	609.31	19.7 m	46.30	0.428	555	0.012	0.422	534	0.003	0.425	554	0.003
	934.06		3.21		7659	0.230		10,737	0.076		8329	0.055
	1155.19		1.69		19,680	0.701		33,759	0.285		21,123	0.166
	1509.19		2.19		103,230	4.650		117,845	1.257		106,523	1.058
	1764.49		15.80		620	0.032		890	0.011	-	-	-
	2118.54		1.21		6882	0.430	-	-	-	-	-	-
^{234m}Pa	1001.03	1.17 m	0.84	0.512	29,378	0.931	-	-	-	-	-	-

* The 'yield' denotes the probability that a gamma photon of a specific energy is emitted per the disintegration of this radionuclide. ** The measurement uncertainty (±5%) was evaluated using the radionuclide identification software (Genie 2000. Gamma Acquisition & Analysis V3.2.1. 26 August 2009, by Canberra Industries), with the activity uncertainties for each radionuclide in (μCi) listed in the Nuclide Identification Report (Supplementary Materials).

The specific activity of the ^{40}K radionuclide in sample 2 is 1.18 times higher than in sample 3 (Table 2), indicating that the foreshore sand may function as a natural filter by retaining radionuclides from seawater as it percolates through the sand. The effectiveness of retention is closely related to the filtering efficiency of seawater, which, in turn, is strongly influenced by the grain size of the sand. Finer sand grains have a larger surface area, which improves radionuclide adsorption and capture [27]. This result is based only on two types of sand: foreshore sand with an average grain diameter of $(5.9 \pm 2.2) \times 10^{-4}$ m, and dune top sand with an average grain diameter of $(2.4 \pm 1.1) \times 10^{-4}$ m. Assuming a spherical grain geometry, the estimated total surface area of the grains in sample 1 (mass 1352.7 g) is approximately 5.19 m^2, whereas in sample 2 (mass 1452.9 g) it is approximately 13.71 m^2. Thus, the coarser sand provides about 2.64 times less surface area than the finer sand, underscoring its lower capacity for radionuclide retention. However, it is important to note that finer grains are also lighter. Based on surface area alone, one might expect lower radionuclide adhesion in the coarser foreshore sand. Contrary to this expectation, the data indicate higher ^{40}K activity in the foreshore sample, suggesting a stronger influence of seawater interaction compared to the top of the dune.

For a more accurate assessment of the filtration properties of sand as a function of grain size, additional sampling is required in multiple locations with varying average grain diameters. It is also essential that the sand within each sample exhibit a high degree of uniformity in grain size to reduce variability and improve comparability.

3.2. Determination of Radionuclide Mass in Analyzed Samples Based on Characteristic Gamma-Ray Emission Spectral Line

The specific gamma activity of a pure radionuclide, A_{pureRN}, can be used as a reference to estimate the mass of each radionuclide present in samples 1 to 3. The mass of a given identified radionuclide in a sample, m_{RN}, can then be calculated using the following expression:

$$m_{\text{RN}} = \frac{A_\gamma}{A_{\text{ pureRN}} \times \text{Sample mass}} \quad (6)$$

where A_γ is the measured specific gamma activity (in Bq·g^{-1}) of the radionuclide in the sample, and A_{pureRN} (in Bq·g^{-1}) is calculated using for following equation:

$$A_{\text{pureRN}} = \frac{N_{\text{A}} \cdot \ln 2}{M_{\text{RN}} \cdot T_{1/2}} \quad (7)$$

Here, $N_{\text{A}} = 6.022 \times 10^{23}$ mol^{-1} is Avogadro's number, M_{RN} is the molar mass (in g·mol^{-1}), and $T_{1/2}$ is the half-life (in seconds) of the specific radionuclide. Based on the intensity of the 1460.80 keV gamma emission line of the ^{40}K radionuclide in samples 1 to 3, the measured specific gamma activities are $A_{\gamma,40_K} = 0.927$ Bq·g^{-1}, 0.251 Bq·g^{-1}, and 0.211 Bq·g^{-1}, as listed in Table 2. Assuming that the specific activity of natural potassium is $A_{\text{K}} = 31.00$ Bq·g^{-1} [28], the corresponding potassium contents in the samples were calculated to be 3.49 mg·kg^{-1}, 0.94 mg·kg^{-1}, and 0.795 mg·kg^{-1}, respectively. The full set of calculated results for ^{40}K and other identified radionuclides, those characterized by the highest spectral line identification confidence and half-lives longer than several days (out of a total of 13 detected in the gamma spectra), are summarized in Table 3.

Some of the radionuclides chosen for the current analysis originate from natural and anthropogenic sources: ^{40}K is a naturally occurring potassium radioisotope that comprises approximately 0.0117% of natural potassium. It enters seawater through the weathering of continental rocks and riverine input, and since potassium is a major ion in seawater, ^{40}K is naturally present wherever potassium occurs. In contrast, several radionuclides found in the samples are of anthropogenic origin: ^{65}Zn is a man-made radionuclide that

can enter the marine environment through discharges from nuclear facilities, industrial waste, or medical sources. ^{106}Ru is produced in nuclear reactors as a fission product. It can persist in the environment and was notably detected in the Baltic Sea following the Chernobyl accident, where it attached to particles and accumulated in sediments and marine organisms. ^{124}I is an artificial radionuclide produced in cyclotrons for medical imaging. ^{137}Cs is a long-lived fission product and one of the most important anthropogenic radionuclides in marine environments. It spreads widely after nuclear releases and has been extensively studied in the Baltic Sea after Chernobyl, where it remains in seawater and sediments and serves as a key tracer of radioactive contamination and environmental transport processes [29].

Table 3. The results of calculations of radionuclide mass from gamma spectra of dried seawater (sample 1), foreshore sand (sample 2), and dune top sand (sample 3) collected in the Juodkrante region in 2021.

Sample	Radionuclide in Sample	Decay Constant λ, s^{-1}	Specific Activity of Pure Radionuclide, $Bq \cdot g^{-1}$	M_{RN}, $g \cdot mol^{-1}$	m_{RN}, $mg \cdot kg^{-1}$
Sample 1	^{40}K	1.760×10^{-17}	2.653×10^{5}	39.964	3.49
Sample 2					0.944
Sample 3					0.795
Sample 1	^{65}Zn	3.283×10^{-8}	3.04×10^{8}	64.929	7.469×10^{-5}
Sample 2					3.036×10^{-5}
Sample 3					1.768×10^{-5}
Sample 1	^{106}Ru	2.147×10^{-8}	1.2×10^{14}	105.907	4.897×10^{-10}
Sample 2					1.115×10^{-10}
Sample 3					1.077×10^{-10}
Sample 1	^{124}I *	1.918×10^{-6}	6.13×10^{14}	123.906	1.669×10^{-11}
Sample 2					0.380×10^{-11}
Sample 3					0.365×10^{-11}
Sample 1	^{137}Cs	7.313×10^{-10}	3.21×10^{12}	136.907	2.192×10^{-9}
Sample 2					0.500×10^{-9}
Sample 3					0.483×10^{-9}

* The line of 1509.49 keV has been used for calculations of the total mass of the ^{124}I radionuclide in samples 1 to 3. Using line 602.71 keV, the mass of a radionuclide in the sample is of two orders in magnitude lower.

A comparison of the values presented in the column "m_{RN}" of Table 3 indicates that seawater contains the highest concentration of radionuclides, while the sand from the top of the dune exhibits the lowest. To quantitatively assess the relative difference in radionuclide concentration between sample 2 (M_{S2}) and sample 3 (M_{S3}), the data of sample 2 were used as a reference. The percentage difference ΔM was calculated using the following expression:

$$\Delta M = \frac{M_{S2} - M_{S3}}{M_{S2}} \times 100\% \quad (8)$$

For radionuclides ^{40}K, ^{65}Zn, ^{106}Ru, ^{124}I, and ^{137}Cs, the calculated differences were 15.9%, 41.9%, 3.4%, 15.8%, and 3.3%, respectively. These results support the hypothesis that the foreshore environment can function as a natural filter, facilitating the accumulation of radionuclides from seawater. In particular, the concentration differences between samples 2

and 3 exceed 10% in most cases, suggesting that such variations can be effectively detected using a portable gamma spectrometer.

3.3. Determination of Radionuclide Concentration in Analyzed Samples Based on Beta-Ray Emissions from Tested Samples

The pulse counting rate for all the tested samples was measured using a beta radiometry setup. These measurements enabled the evaluation of the correlation between beta-emitting radionuclide concentrations in different environments: seawater (sample 1), foreshore sand (sample 2), and dune top sand (sample 3). Background radiation was averaged from three count records lasting approximately 1 h and subtracted from the sample data to ensure accuracy. The mass of the sample was determined by weighting the filled container and subtracting the mass of the empty container. Estimate the total beta activity of radionuclides within a sample. It was assumed that the beta radiation from the sample is detected only within an approximate angle of $\Omega(R)$~70° out of 360 (Figure 4), and that the air attenuation factor for beta particles is approximately 0.8 (i.e., approximately 20% of the beta particles emitted by the sample are lost due to air attenuation before reaching the detector). On the basis of these assumptions, the total beta activity was calculated using the following relationship:

$$A_{\text{Total}} = \frac{N}{\eta_{\beta} \cdot 0.8}. \quad (9)$$

Here, N is the total number of counts, which is equal to the product of counts registered by the detector by a rate of 360/70 = 5.14, which allows us to take into account the missing detector counts emitted from the sample, η_{β} = 0.3 is detector efficiency, and 0.8 is an air attenuation factor. The data of these calculations are presented in the last column of Table 4 for sample 1 (dried seawater), sample 2 (foreshore sand), and sample 3 (sand on the top of the dune). An air attenuation correction factor of 0.8 was applied, accounting for an estimated 20% loss of β-particles due to absorption in air before reaching the detector.

Table 4. The β-particle pulse counts and specific β-activity values of samples 1 to 3 collected in the Juodkrante region between 2019 and 2024 (as previously reported in Table 1).

Sample	Date of Sampling	Sample Mass, g	Measurement Duration, s	β-Particle Pulse Count	Specific β-Activity A_{β}, Bq·kg^{-1}
Sample 1	15 June 2019	8.3	86,880	89,983.57	45.17
	30 May 2020	8.52	54,480	64,896.99	31.74
	9 June 2021	8.68	60,600	72,045.49	34.58
	14 June 2022	9.66	70,260	91,932.69	39.65
	19 May 2023	9.44	25,560	30,193.38	13.33
	17 June 2024	9.44	90,540	87,489.31	38.62
Sample 2	15 June 2019	18.76	-	-	-
	30 May 2020	-	-	-	-
	9 June 2021	20.24	41,640	52,744.56	10.86
	14 June 2022	18.3	28,500	31,345.37	7.14
		17.52	62,640	67,632.96	16.08
		19.18	70,080	79,687.69	17.31
	19 May 2023	17.06	19,200	17,876.37	4.37
		19.68	67,860	81,677.95	17.29
		20.78	97,260	121,118.08	24.29
		20.54	50,040	59,821.05	12.14
	17 June 2024	18.76	27,240	30,728.23	6.82
		19.82	16,320	14,749.55	3.10

Table 4. *Cont.*

Sample	Date of Sampling	Sample Mass, g	Measurement Duration, s	β-Particle Pulse Count	Specific β-Activity A_β, $Bq \cdot kg^{-1}$
Sample 3	15 June 2019	-	-	-	-
	30 May 2020	-	-	-	-
	9 June 2021	19.92	16,200	17,259.24	3.61
	14 June 2022	17.53	15,180	15,402.69	3.66
	19 May 2023	18.10	82,980	86,090.47	19.82
	17 June 2024	19.52	44,820	53,063.41	11.33

By comparing the data presented Tables 1 and 4, it is evident that the specific activity of the samples follows a consistent pattern. While seawater samples generally exhibit the highest radionuclide concentrations, attributable in part to their significantly large sample volumes (typically ten or more times greater than those of sand), the foreshore sand frequently shows higher specific activities than the dune top sand. This observation supports the hypothesis that foreshore sand can serve as a proxy for assessing radionuclide concentrations in seawater, not only at the time of sampling but also retrospectively. For example, in 2021, the specific beta-activity of the foreshore sand (sample 2) was 10.86 $Bq \cdot kg^{-1}$, compared to 3.61 $Bq \cdot kg^{-1}$ in the dune top sand (sample 3), indicating a nearly threefold difference. This suggests that radionuclides from seawater may accumulate in foreshore sand due to repeated inundation and deposition driven by wave action. However, it must also be noted that wave dynamics, such as strong backwash and sediment transport, can lead to erosion and the removal of radionuclide-bearing sand from the foreshore. As a result, there is a risk that the radionuclide concentrations measured at the time of sampling may underestimate actual values due to recent sediment displacement.

On the other hand, the seawater can infiltrate deeply into the foreshore sand [22], suggesting that the highest concentration of radionuclides may not be found at the surface, but rather at depths approaching the local groundwater table. This level is governed by the principle of communicating vessels, where one level corresponds to the seawater and the other to the water within the saturated foreshore sand, which is regularly flooded by wave action. Figure 6 illustrates the dependence of radionuclide β-activity on sampling depth. The data were obtained from sand samples collected at the same location, but at various depths down to approximately 60 cm, extending to the depth where seawater saturates the foreshore sand.

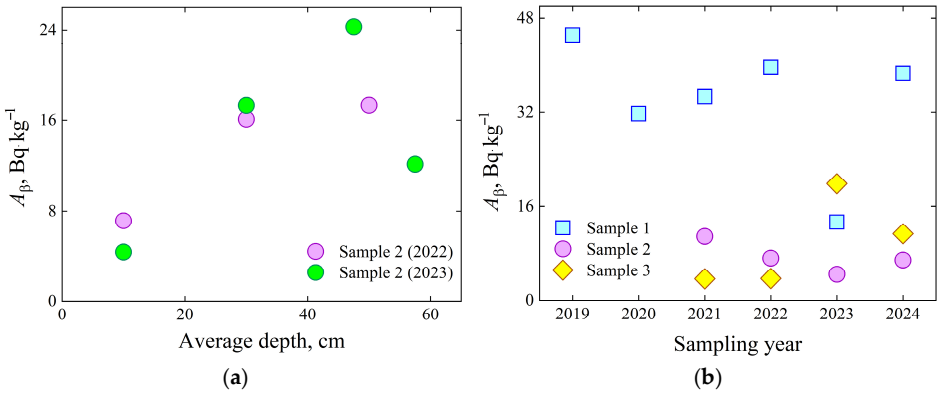

Figure 6. The specific beta-activity values determined using a beta radiometry setup (**a**) measured in foreshore sand (sample 2) during the period of 2002–2023 at various depths ranging from 10 to 60 cm and (**b**) the variation in beta-activity in samples 1 to 3, collected during the period of 2019–2024 for samples 1 to 3.

The variation in A_β versus the average depth of sampling confirms that due to frequent interaction with receding waves, the sand radioactivity on the surface of the foreshore can be washed with seawater, or sand that was not in frequent contact with seawater can replace the foreshore sand removed by waves. Some of the water carried by the wave immediately returns to the sea, carrying the sand from the foreshore, but some of it is absorbed into the sand, leaving radioactive particles in it. Considering that the water absorbed into the sand returns to the sea only through diffusion through the grains of the sand, it is likely that it can leave the contaminants it contains, including radionuclides, in the sand located deeper than the shore. This hypothesis is confirmed by the data shown in Figure 6a, which indicate that the highest concentration of radionuclides at this sampling site appears to be 0.45–0.5 m from the surface. At this depth, the seawater that penetrated through the sand granules is at the level of communicating vessels. The depth of the highest concentration of radionuclides depends on the distance from the coast and the steepness of the sandy coast. For the foreshore sand sampling, the distance from the coast was chosen in the range of 2 to 6 m, where the foreshore sand becomes wet from depths of approximately 0.1 m and continues throughout the entire sampling depth.

To obtain more robust evidence of the correlation between A_β measured in dried seawater and foreshore surface sand samples, a longer observational period, exceeding six years, is necessary. Furthermore, it is important to select some specific foreshore sites with natural barriers that limit the redistribution of sand caused by wave backwash, since episodic deposition and erosion events, such as those driven by sudden storms or dune erosion [30], can significantly alter the distribution of radionuclides. The processes mentioned above may contribute to the weak correlation between A_β activity in sample 1 and sample 2 (Figure 6b).

Despite this, the proposed method shows promise. By measuring beta-activity in the foreshore sand at varying distances from the shoreline, it is possible to infer wave amplitude and flood frequency at specific sites. Each storm event introduces radionuclides from seawater, and naturally occurring beta emitters such as ^{40}K, ^{238}U, or ^{226}Ra can accumulate in the foreshore sand, effectively turning it into a passive indicator of changes in seawater radioactivity over time. The proposed method for investigating and monitoring seawater quality reduces the need to collect and process large volumes of seawater, which typically requires evaporation and salt concentration for radionuclide analysis. In particular, the evaporation and drying step can lead to the loss of volatile radionuclides, reducing the accuracy of the measurement. By avoiding these issues, the proposed method saves time, energy, and labor. These efficiencies make the approach more practical for long-term monitoring and offer a sustainable solution for assessing radionuclide contamination in marine and freshwater coastal environments containing foreshore sand affected by wave action.

4. Conclusions

The results demonstrate that radionuclides can be retained in sandy substrates long after episodic seawater contamination events, with retention influenced by both hydrodynamic and aeolian processes. Monitoring radionuclide contamination in foreshore sand therefore presents a sustainable and practical approach to assessing long-term contamination in marine coastal environments.

Gamma and beta activity measurements indicate that radionuclide concentrations in the foreshore sand vary with both the distance from the shoreline and the depth. The zone of maximum accumulation of radionuclides reflects the influence of slow seawater movement and the natural filtration capacity of the sand, underscoring the role of the foreshore as an effective sink for radionuclide contaminants. These findings are original in

that they consistently confirm higher radioactivity in the foreshore sand compared to the reference sample (sand on top of the dune), thus validating the hypothesis of this study regarding the accumulation of radionuclides from seawater.

The sampling of foreshore sand near water sampling sites can serve as a valuable proxy for assessing seasonal radionuclide pollution, particularly when direct water sampling is limited or not feasible, such as in freshwater bodies. This complementary method can improve temporal resolution and offer a more comprehensive understanding of long-term radionuclide dynamics in coastal zones of large waterbodies influenced by wave action.

To better understand how grain size affects sand filtration, more samples are needed from sites with different but more uniform grain sizes. Still, a well-characterized coastal site can reliably indicate seawater pollution, especially from radionuclides. In this study, a Juodkrante site was chosen on the basis of stable shoreline and wave conditions, which influence the transport of contaminants. Waves bring polluted water to shore, where the sand filters and retains radionuclides, particularly in the upper layers. The sampling in the wave-flooded zone (1–7 m from the waterline) captures recent contamination. Comparing these samples with dune sand, which is unaffected by waves, helps identify trends, making this method also useful for monitoring regional pollution.

Supplementary Materials: The following supporting information can be downloaded at https://www.mdpi.com/article/10.3390/su17167441/s1; Data Sheet S1: The gamma spectrum and results of analysis for the dried seawater (sample 1) collected in Juodkrante in June 2021; Data Sheet S2: The gamma spectrum and results of analysis for the foreshore sand (sample 2) collected in Juodkrante in June 2021; Data Sheet S3: The gamma spectrum and results of analysis for the dune top sand (sample 3) collected in Juodkrante in June 2021.

Author Contributions: Conceptualization, A.J.; methodology, A.J.; formal analysis, A.J. and G.G.-V.; investigation A.J.; writing—original draft preparation, A.J.; writing—review and editing, A.J. and G.G.-V.; supervision, A.J. All authors have read and agreed to the published version of the manuscript.

Funding: This research received no external funding.

Institutional Review Board Statement: Not applicable.

Informed Consent Statement: Not applicable.

Data Availability Statement: Data is contained within the article and Supplementary Materials.

Conflicts of Interest: The authors declare no conflicts of interest.

References

1. Biswas, R.; Sahadath, H.; Mollah, A.S.; Hug, M.F. Calculation of gamma-ray attenuation parameters for locally developed shielding material: Polyboron. *J. Rad. Res. Appl. Sci.* **2016**, *9*, 26–34. [CrossRef]
2. Joseph, J.M.; Choi, B.S.; Yakabuskie, P.; Wren, J.C. A combined experimental and model analysis on the effect of pH and O_2(aq) on γ-radiolytically produced H_2 and H_2O_2. *Rad. Phys. Chem.* **2008**, *77*, 1009–1020. [CrossRef]
3. Stalter, R.; Howarth, D. Gamma Radiation (Chapter III). In *Gamma Radiation*; Adrovic, F., Ed.; IntechOpen: Rijeka, Croatia, 2012; pp. 154–196.
4. Uddin, M.G.; Rahman, A.; Sajib, A.M.; Nash, S.; Diganta, M.T.M.; Sajib, A.M.; Moniruzzaman, M.; Olbert, A.I. Marine waters assessment using improved water quality model incorporating machine learning approaches. *J. Environ. Manag.* **2023**, *344*, 118368. [CrossRef] [PubMed]
5. Arctic Monitoring and Assessment Programme (AMAP). Radioactivity (Chapter 8). In *AMAP Assessment Report: Arctic Pollution Issues*; Arctic Monitoring and Assessment Programme (AMAP): Tromsø, Norway, 1998; pp. 525–615.
6. Omar-Nazir, L.; Shi, X.; Moller, A.; Mousseau, T.; Byun, S.; Hancock, S.; Seymour, C.; Mothersill, C. Long-term effects of ionizing radiation after the Chernobyl accident: Possible contribution of historic dose. *Environ. Res.* **2018**, *165*, 55–62. [CrossRef]
7. Vuorinen, I.; Hänninen, J.; Rajasilta, M.; Laine, P.; Eklund, J.; Montesino-Pouzols, F.; Corona, F.; Junker, K.; Markus Meier, H.E.; Dippner, J.W. Scenario simulations of future salinity and ecological consequences in the Baltic Sea and adjacent North Sea areas–implications for environmental monitoring. *Ecol. Indic.* **2015**, *50*, 196–205. [CrossRef]

8. Bezhin, N.B.; Milyutin, V.V.; Kuzmenkova, N.V.; Shibetskaia, I.G.; Kozlovskaia, O.N.; Slizchenko, E.V.; Razina, V.A.; Tananaev, I.G. Radionuclides' Recovery from Seawater Using FIC and FIC A Sorbents. *Materials* **2023**, *16*, 4181. [CrossRef]
9. Styro, D.; Morkūnienė, R.; Daunaravičienė, A. On variations of volumetric activity of ^{90}Sr and ^{137}Cs in the Baltic Sea coastal waters near the shore of Lithuania in 2005–2009. *J. Radioanal. Nucl. Chem.* **2012**, *293*, 923–929. [CrossRef]
10. Van Beek, P.; Souhaut, M.; Reyss, J.L. Measuring the radium quartet (^{228}Ra, ^{226}Ra, ^{224}Ra, ^{223}Ra) in seawater samples using gamma spectrometry. *J. Environ. Radioact.* **2010**, *101*, 521–529. [CrossRef] [PubMed]
11. Holtermann, P.L.; Prien, R.; Naumann, M.; Mohrholz, V.; Umlauf, L. Deepwater dynamics and mixing processes during a major inflow event in the central Baltic Sea. *J. Geophys. Res. Ocean.* **2017**, *122*, 6648–6667. [CrossRef]
12. Håkanson, L.; Bryhn, A.C. Water Exchange and Water Transport in the Baltic Sea (Chapter III). In *Eutrophication in the Baltic Sea*, 1st ed.; Springer: Berlin/Heidelberg, Germany, 2008; pp. 69–89.
13. Kelpšaitė, L.; Herrmann, H.; Soomere, T. Wave regime differences along the eastern coast of the Baltic Proper. *Oceanography* **2008**, *57*, 225–231. [CrossRef]
14. Uścinowicz, S.; Jegliński, W.; Miotk-Szpiganowicz, G.; Nowak, J.; Pączek, U.; Przezdziecki, P.; Szefler, K.; Poręba, G. Impact of sand extraction from the bottom of the southern Baltic Sea on the relief and sediments of the seabed. *Oceanologia* **2014**, *56*, 857–880. [CrossRef]
15. Weisse, R.; Dailidienė, I.; Hünicke, B.; Kahma, K.; Madsen, K.; Omstedt, A.; Parnell, K.; Schöne, T.; Soomere, T.; Zhang, W.; et al. Sea level dynamics and coastal erosion in the Baltic Sea region. *Earth Syst. Dynam.* **2021**, *12*, 871–898. [CrossRef]
16. Madsen, K.S.; Høyer, J.L.; Suursaar, Ü.; She, J.; Knudsen, P. Sea Level Trends and Variability of the Baltic Sea From 2D Statistical Reconstruction and Altimetry. *Front. Earth Sci.* **2019**, *7*, 243. [CrossRef]
17. Copplestone, D.; Johnson, M.S.; Jones, S.R. Behaviour and transport of radionuclides in soil and vegetation of a sand dune ecosystem. *J. Environ. Radioact.* **2001**, *55*, 93–108. [CrossRef] [PubMed]
18. Druteikiene, R.; Morkuniene, R.; Luksiene, B. Distribution of artificial radionuclides in the Baltic seaside environment. *Lith. J. Phys.* **2011**, *51*, 75–81. [CrossRef]
19. Eakins, J.D.; Lally, A.E.; Burton, P.J.; Kilworth, D.R.; Pratley, F.A.; UKAEA Atomic Energy Research Establishment, Harwell. *Studies of Environmental Radioactivity in Cumbria. Part 5. The Magnitude and Mechanism of Enrichment of Sea Spray with Actinides in West Cumbria*; UKAEA Atomic Energy Research Establishment, Harwell: Oxfordshire, UK; Environmental and Medical Sciences Div.: Durham, NC, USA, 1982; Version 1. Available online: https://inis.iaea.org/records/9as8s-82b16 (accessed on 5 March 2025).
20. Eakins, J.D.; Cambray, R.S.; UKAEA Atomic Energy Research Establishment, Harwell. *Studies of Environmental Radioactivity in Cumbria*; Environmental and Medical Sciences Div.: Durham, NC, USA, 1985; Version 1. Available online: https://inis.iaea.org/records/fs891-hwn22 (accessed on 5 March 2025).
21. Heijmansa, K.; Holkenborga, B.K.; Gaastra-Nedea, S.; Smeulders, D. Advanced diffusion methods for H_2O in salt hydrates. *Computat. Mat. Sci.* **2022**, *205*, 111154. [CrossRef]
22. Iaffaldano, G.; Caputo, M.; Martino, S. Experimental and theoretical memory diffusion of water in sand. *Hydrol. Earth Syst. Sci.* **2006**, *10*, 93–100. [CrossRef]
23. Sosa, M.A.; Zega, C.J.; Villagran Zaccardi, Y.A. A comparative study assessing the validity of water absorption methods when applied to secondary fine aggregates. *Constr. Build. Mater.* **2024**, *432*, 136590. [CrossRef]
24. Jay-Gerin, J.-P. Fundamentals of water radiolysis. *Encyclopedia* **2025**, *5*, 38. [CrossRef]
25. Herrmann, J.; Hutri, K.-L.; Ikäheimonen, T.K.; Kanisch, G.; Lüning, M.; Nielsen, S.P.; Pham, M.K.; Vartti, V.-P. *Thematic Assessment of Long-Term Changes in Radioactivity in the Baltic Sea, 2007–2010*; Baltic Sea Environment Proceedings No. 135; Helsinki Commission: Helsinki, Finland, 2013; p. 16. Available online: https://helcom.fi/wp-content/uploads/2019/08/BSEP135.pdf (accessed on 20 June 2025).
26. Skowron, P.; Skowrońska, M.; Bronowicka-Mielniczuk, U.; Filipek, T.; Igras, J.; Kowalczyk-Juśko, A.; Krzepiłko, A. Anthropogenic sources of potassium in surface water: The case study of the Bystrzyca river catchment, Poland. *Agric. Ecosyst. Environ.* **2018**, *265*, 454–460. [CrossRef]
27. Onwuka, M.; Ononugbo, C.; Ikirigo, J. Effect of grain size on radionuclide content in sediment samples from Kolo Creek, Bayelsa state, Nigeria. *Asien J. Res. Rev. Phys.* **2023**, *7*, 25–34. [CrossRef]
28. Samat, S.B.; Green, S.; Beddoe, A.H. The ^{40}K activity of one gram of potassium. *Phys. Med. Biol.* **1997**, *42*, 407–413. [CrossRef] [PubMed]

29. Herrmann, J.; Ikäheimonen, T.K.; Ilus, E.; Kanisch, G.; Lüning, M.; Mattila, J.; Nielsen, S.P.; Osvath, I.; Outola, I. *Radioactivity in the Baltic Sea, 1999–2006. HELCOM Thematic Assessment*; Baltic Sea Environment Proceedings No. 117; Baltic Marine Environment Protection Commission, Helsinki Commission: Helsinki, Finland, 2009; p. 7. Available online: https://helcom.fi/wp-content/uploads/2019/08/BSEP117.pdf (accessed on 24 July 2025).
30. Kaehler, C.; Cantré, S.; Schweiger, C.; Saathoff, F. Dune erosion at the German Baltic coast—Investigation and analysis of a large-scale field experiment compared to life dunes. *J. Mar. Sci. Eng.* **2022**, *10*, 1605. [CrossRef]

Disclaimer/Publisher's Note: The statements, opinions and data contained in all publications are solely those of the individual author(s) and contributor(s) and not of MDPI and/or the editor(s). MDPI and/or the editor(s) disclaim responsibility for any injury to people or property resulting from any ideas, methods, instructions or products referred to in the content.